

GT2011-45(, *

SIMULATION OF CONFINED CO-FLOW METHANE-AIR DIFFUSION FLAME UNDER MICROGRAVITY CONDITION WITH VARIABLE PROPERTY FORMULATION

Manjula Das (Ghatak), Sujoy Kumar Mukherjea

Department of Aerospace Engineering and Applied Mechanics
Bengal Engineering and Science University, Shibpur, Howrah 711109, INDIA

And

Bijan Kumar Mandal

Department of Mechanical Engineering,
Bengal Engineering and Science University, Shibpur, Howrah 711109, INDIA

ABSTRACT

Numerical computations have been conducted to study the responses of laminar diffusion flames produced by combustion of methane and air under different microgravity conditions. The combustion process is simulated with a detailed numerical model, solving the governing equations of mass, momentum, energy and species conservations with appropriate boundary conditions. The numerical code for the reacting flow is validated by comparing radial distribution of temperature and major product species (CO_2 and H_2O) concentrations at an axial height of 12 mm above the burner rim against experimental data available in the literature for normal gravity condition. The temperature data as well as the species distributions of the combustion products predicted by the present code show good agreement with the experiments. The result of the numerical simulation is presented for air inlet temperatures 300 K and the fuel inlet temperature 300 K under normal gravity, 75% of gravity, 50% of gravity, 25% of gravity and zero gravity. The preliminary investigation of temperature distribution at normal gravity shows a very high temperature gradient at the base of the flame and higher isotherms near the axis. As the gravity level is decreased the isotherms gradually move away from the axis and get scattered in the computation domain. In the zero gravity level, the isotherms are uniformly distributed in the computation domain. The flame structure is further illustrated from the velocity distribution where it is seen that at normal gravity there is entrainment of flow from the co-flowing air into the flame zone. There is acceleration in the central region due to the effects of high temperature and gravity, which further augments the entrainment process. A stable recirculation zone near the wall is observed at normal gravity condition. As the gravity level decreases the entrainment of flow from the co-flowing air into the flame zone decreases and gradually the recirculation zone decreases. Finally, at zero gravity condition recirculation zone disappears completely.

INTRODUCTION

Combustion theory is one of the most elegant areas of classical phenomenology, presenting a wide range of natural phenomenon that can be deduced from a few fundamental principles [1]. In combustion, there is a strong coupling among transport (heat transfer, molecular diffusion, convection, turbulent transport) and chemistry and hence it is a multidisciplinary topic of research. Sometimes, the effects of gravity are undesirable in understanding certain physical, chemical or biological phenomena or studying the complex interaction of different forces involved in a process. Gravity is also undesirable in certain industrial production processes. Now-a-days, the study of combustion under microgravity condition has extended the understanding of combustion science by providing gravity-free means to unravel important physical and chemical processes, boosted by space exploration mission. As an important branch of combustion research, microgravity combustion is of great importance, both in academic research and in practical application. Similar as earth's normal gravity combustion systems, most microgravity combustion systems fall into two categories, premixed and non-premixed (diffusion) combustion. Laminar gas jet diffusion flames are fundamental to combustion and they account for the majority of practical combustion systems. Since the buoyancy effect could be neglected in a microgravity field, a large number of studies on microgravity combustion have been performed to simplify the combustion phenomena by using a drop tower or parabolic flight aircraft. Edelman and coworkers [2-4] and Sunderland et al. [5] investigated the flame shape under microgravity conditions obtained in the NASA Lewis 2.2-s drop tower. Edelman et al. [2] observed that the flame length under microgravity condition was longer than that in normal-gravity experiments. Sunderland et al. [5] measured the shapes of buoyant and nonbuoyant laminar jet diffusion flames. They

showed that their results agreed with those of Edelman et al. Lin et al. [6] investigated the shapes of laminar jet diffusion flames obtained on orbit in the space shuttle Columbia. They observed the flame at the various ambient pressures and jet exit Reynolds numbers, and compared the experimental data with the theoretical analyses. Kim et al. [7] investigated characteristics of oscillating lifted flames numerically and experimentally by varying the gravity level in co-flow jets using propane fuel highly diluted with nitrogen and found that the oscillation amplitude and frequency increased with gravity level. As the gravity level decreased, the oscillation ceased and stationary lifted flames were stabilized when the gravity level became smaller than a critical value. Lee et al. [8] investigated the propagation speed of tribrachial (triple) flames in laminar propane jets, experimentally under normal and micro gravity conditions and found that the displacement speed varied nonlinearly with axial distance because the flow velocity along the stoichiometric contour was comparable to the propagation speed of tribrachial flame. Yuan et al. [9] demonstrated that in a microgravity environment, produced using a drop tower facility, a spherically symmetric flame configuration can be established, where the flame becomes one-dimensional and the flow field is co-linear with the electric field.

Diffusion flame has applications in gas turbine and diesel engines. Although the literature is rich in combustion under normal gravity level, there is a lack of study of combustion phenomenon in diffusion mode under microgravity conditions. The knowledge of the temperature and velocity distributions in a diffusion flame is essential for the understanding of different physical and chemical processes took place within the flame. In this paper, the results of the numerical simulation of methane-air diffusion flame are presented for air inlet temperature of 300 K and the fuel temperature of 300 K under microgravity condition.

PHYSICAL MODEL AND THE BASIC EQUATIONS

The combustion system considered in this work is the laminar diffusion flame in a confined physical environment with coflowing fuel and air (oxidizer) streams. The physical model represents a burner consisting of two concentric tubes. The fuel (methane) is admitted as a central jet through the inner tube and air as a co-flowing annular jet through the outer tube. The inner fuel tube diameter is 12.7 mm and the outer tube diameter is 50.4 mm. The inner tube wall is considered to be thin and its thickness is neglected for the computation. The two streams diffuse into each other at the outlet of the inner tube in order to produce a flammable mixture of fuel and air. A schematic diagram of the burner and the flame geometry is shown in the Fig. 1.

As the geometry is an axi-symmetric one, the conservation equations will have the transient term and r and z components of different variables only. The governing equations considered for the present formulation are based on the conservation of mass, radial momentum and axial momentum. The governing equations in cylindrical co-ordinates can be written as:

Conservation of mass:

$$\frac{\partial \rho}{\partial t} + \frac{1}{r} \frac{\partial}{\partial r} (r \rho v_r) + \frac{\partial}{\partial z} (\rho v_z) = 0 \quad (1)$$

Conservation of radial momentum:

$$\frac{\partial}{\partial t} (\rho v_r) + \frac{1}{r} \frac{\partial}{\partial r} (r \rho v_r^2) + \frac{\partial}{\partial z} (\rho v_r v_z) = -\frac{\partial p}{\partial r} + \frac{2}{r} \frac{\partial}{\partial r} \left(r \mu \frac{\partial v_r}{\partial r} \right) - \frac{2}{r} \mu \frac{v_r}{r^2} + \frac{\partial}{\partial z} \left\{ \mu \left(\frac{\partial v_z}{\partial r} + \frac{\partial v_r}{\partial z} \right) \right\} - \frac{2}{3} \frac{\partial}{\partial r} \left\{ \mu \left(\frac{\partial v_r}{\partial r} + \frac{v_r}{r} + \frac{\partial v_z}{\partial z} \right) \right\} \quad (2)$$

Conservation of axial momentum:

$$\frac{\partial}{\partial t} (\rho v_z) + \frac{1}{r} \frac{\partial}{\partial r} (r \rho v_r v_z) + \frac{\partial}{\partial z} (\rho v_z^2) = -\frac{\partial p}{\partial z} + \frac{1}{r} \frac{\partial}{\partial r} \left\{ r \mu \left(\frac{\partial v_z}{\partial r} + \frac{\partial v_r}{\partial z} \right) \right\} + 2 \frac{\partial}{\partial z} \left(\mu \frac{\partial v_z}{\partial z} \right) - \frac{2}{3} \frac{\partial}{\partial z} \left\{ \mu \left(\frac{\partial v_r}{\partial r} + \frac{v_r}{r} + \frac{\partial v_z}{\partial z} \right) \right\} + \rho g \quad (3)$$

The last term on the right hand side of the above equation represents the gravity effect in the axial (vertical) direction.

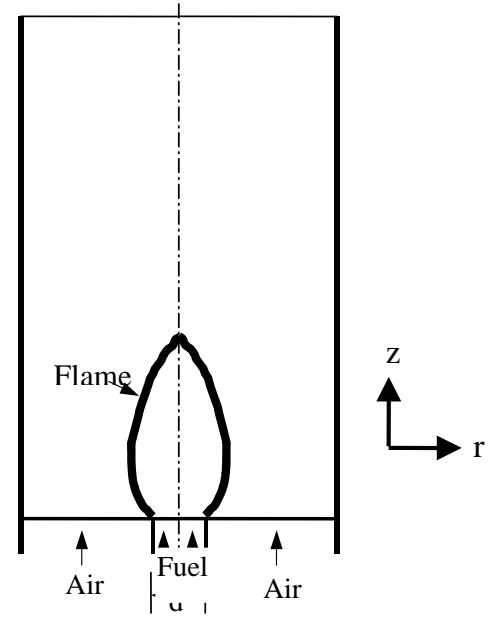
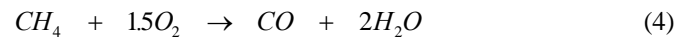


Fig. 1. Schematic diagram of the burner and the flame geometry

The combustion of methane and air takes place through different reaction steps. For the simplification of the problem, the combustion reaction of methane and air is assumed to proceed through simplified two steps reaction. The reactions considered are as follows:



The reaction rates for the above reactions are obtained following an Arrhenius type rate equation, given as

$$\dot{\omega} = A\rho^{\left(\sum_j a_j\right)} \frac{\prod_j C_j^{a_j}}{\prod_j M_j^{a_j}} \exp\left(-\frac{E}{RT}\right) \quad (6)$$

Where, A and E are the pre-exponential factor and activation energy respectively for the respective equations and a_j is the reaction order in terms of j th reactant species. The values for these parameters are taken from the work of DuPont et al. [10].

The conservation equation for chemical species is solved for five gaseous species, viz. CH₄, O₂, CO₂, CO and H₂O. The concentration for N₂ is obtained by difference. The governing equation for the gaseous species conservation is as follows:

$$\frac{\partial}{\partial t}(\rho C_j) + \frac{1}{r} \frac{\partial}{\partial r}(r\rho v_r C_j) + \frac{\partial}{\partial z}(\rho v_z C_j) = \frac{1}{r} \frac{\partial}{\partial r}\left(r\rho D_{jm} \frac{\partial C_j}{\partial r}\right) + \frac{\partial}{\partial z}\left(\rho D_{jm} \frac{\partial C_j}{\partial z}\right) + \dot{S}_{cj} \quad (7)$$

Where, C_j is the mass fraction of the respective species and D_{jm} is the diffusion coefficient of the species in a binary mixture of that species and nitrogen as described by Katta et al. [11]. The source term \dot{S}_{cj} is the rate of production or destruction of the species j per unit volume due to chemical reaction. The source terms are calculated as

$$\dot{S}_{cj} = \sum_{k=1}^2 (\gamma_{jk}^r \dot{\omega}_k - \gamma_{jk}^r \dot{\omega}_k) M_j \quad (8)$$

Where, M_j is the molecular weight of the j th species. γ_{jk}^r and γ_{jk}^r are the stoichiometric coefficients on the product side and reactant side respectively for the j th species in the k th reaction. Obviously, for the present simple reaction mechanism, k is either 1 for the reaction given by Eq. (4) or 2 for the reaction given by Eq. (5). The density of the species mixture is calculated using the equation of state considering all the species as ideal gases. The enthalpy for chemically reacting flow is given as the weighted sum of each mass fraction according to the following relation:

$$h = \sum_{j=1}^n C_j h_j = \sum_{j=1}^n C_j \left(h_{fj}^0 + \int_{T_0}^T c_{pj} dT \right) \quad (9)$$

Where, h_{fj}^0 is the heat of formation of the j th species at the reference temperature T_0 and the integral part is the contribution of the sensible heat.

The energy equation for the reaction flow is written as

$$\frac{\partial}{\partial t}(\rho h) + \frac{1}{r} \frac{\partial}{\partial r}(r\rho v_r h) + \frac{\partial}{\partial z}(\rho v_z h) = \frac{1}{r} \frac{\partial}{\partial r}\left(r \frac{\lambda}{c_p} \frac{\partial h}{\partial r}\right) + \frac{1}{r} \frac{\partial}{\partial r}\left[r \frac{\lambda}{c_p} \sum_{j=1}^n h_j (Le_j^{-1} - 1) \frac{\partial C_j}{\partial r}\right] + \frac{\partial}{\partial z}\left[\frac{\lambda}{c_p} \sum_{j=1}^n h_j (Le_j^{-1} - 1) \frac{\partial C_j}{\partial z}\right] \quad (10)$$

Le_j in the above equation is the local Lewis number of the j th species defined as

$$Le_j = \frac{\lambda}{c_p \rho D_{jm}} \quad (11)$$

The last two terms in the energy equation are caused by the preferential diffusion of species in the radial and axial directions respectively. The specific heat c_p is a strong function of temperature and is locally calculated for each species at the respective temperature. The mixture specific heat is then calculated considering an ideal gas mixture. The temperature of the gas mixture is implicitly calculated by solving Eq.(9) using Newton-Raphson method. The solution is refined until the accuracy within the prescribed criteria (i.e. 0.003%) is achieved.

The transport of momentum, energy and species mass in the calculation of a reacting flow involve the transport coefficients like viscosity (μ), thermal conductivity (λ) and mass diffusivity (D_{jm}) for the mixture. The local viscosity of the species j is computed from the local temperature using a power law as,

$$\mu_j = \mu_j^0 \left(\frac{T}{T_0}\right)^p \quad (12)$$

μ_j^0 represents the reference viscosity of species j at the reference temperature T_0 . The power exponent p is taken as 0.7, in conformity with the earlier work of Smooke et al. [12]. The viscosity of the mixture is calculated using the semi-empirical method of Wilke, as described in Reid et al. [13].

The local thermal conductivity of species j is evaluated using a polynomial expression of thermal conductivity of pure substance as

$$\lambda_j = A_j + B_j T + C_j T^2 + D_j T^3 \quad (13)$$

Where, A_j , B_j , C_j , and D_j are the coefficients for species j , which are taken from Reid et al. [13]. The mixture thermal conductivity is again evaluated using the method of Wilke.

The mass diffusivity, D_{jm} for species j in a binary mixture of j and nitrogen is evaluated using a power law [14] as

$$D_{jm} = D_{jm}^0 \left(\frac{T}{T_0}\right)^{1.5} \quad (14)$$

BOUNDARY CONDITIONS

Boundary conditions at the inlet are given separately for the fuel stream at the central jet and the air stream at the annular co-flow. The streams are considered to enter the computational domain as plug flow, with velocities calculated from their respective mass flow rates. The temperatures of fuel and air along with their thermo physical properties at the inlet are specified. In conformation with the conditions used by Mitchell et al. [15] and Smooke et al. [12], the fuel flow rate is taken as 3.71×10^{-6} kg/s and the airflow rate is taken as 2.214×10^{-4} kg/s. Considering the length of the computational domain to be 0.3 m, the fully developed boundary conditions for the variables are considered at the outlet. In case of reverse flow at the outlet plane, which occurs in the case of buoyant flame, the stream coming in from the outside is considered to be ambient air. Axi-symmetric condition is considered at the central axis, while at the wall a no-slip, adiabatic and impermeable boundary condition is adopted. The boundary conditions imposed for the different parameters at the known locations of the computational domain can be summarized as

At inlet ($z = 0$)

For $r < d_f/2$ (for inner fuel jet),

$$\rho = \rho_f, v_r = 0, v_z = v_f, T = T_f$$

$$C_f = 1, C_O = 0, C_C = 0, C_{CO} = 0, C_W = 0$$

For $r > d_f/2$ (for annular air jet),

$$\rho = \rho_a, v_r = 0, v_z = v_a, T = T_a$$

$$C_f = 0, C_O = 0.232, C_C = 0, C_{CO} = 0, C_W = 0$$

At outlet ($z = L$)

$$v_r = \frac{\partial v_z}{\partial z} = \frac{\partial T}{\partial z} = \frac{\partial C_j}{\partial z} = 0$$

At the axis ($r = 0$), following the conditions of radial symmetry,

$$v_r = 0$$

$$\frac{\partial \rho}{\partial r} = \frac{\partial v_z}{\partial r} = \frac{\partial T}{\partial r} = \frac{\partial C_j}{\partial r} = 0$$

At wall ($r = R$)

$$v_r = v_z = 0$$

$$\frac{\partial T}{\partial r} = \frac{\partial C_j}{\partial r} = 0$$

Though zero axial gradients are prescribed at the exit boundary, in presence of recirculation, the composition and temperature of the fluid entering the computational domain at the exit plane are specified as those the ambient air having temperature 300 K. The outlet boundary conditions for velocity temperature and species concentrations are in agreement with those taken by Smooke et al. [12] for their numerical calculation of a laminar diffusion flame at normal gravity condition.

The methane-air diffusion flame is simulated under different gravity conditions with fuel temperature of 300 K and air temperature of also 300 K. The fuel and air jet velocities at the inlet calculated from the mass flow rates are calculated to be 4.5 cm/s and 9.88 cm/s respectively. The gravity levels considered for the present study are normal gravity (1.0G), 75% (0.75G), 50% (0.50G), 25% (0.25G) of normal gravity and zero gravity (0.0G).

VALIDATION OF THE NUMERICAL CODE

An extensive grid independence test is carried out by several variations of the number of grids in either direction. It is observed that the increase in the numbers of grids from 85×41 to 121×61 almost doubles the computation time, but the maximum change in results is within 2%. Hence a numerical mesh with 85×41 grid nodes is finally adopted.

The numerical code developed for the present work is based on SOLA algorithm for the reacting flow. The code is validated by comparing the predictions against experiments conducted by Mitchell et al. [15] within the flame for the same input and operating conditions. Radial distributions of temperature and major product species (CO_2 and H_2O) concentrations at a height of 12 mm above the burner rim are compared. The temperature values in the high temperature regions are overpredicted by 50-100 K. This may be attributed to the fact that the present model has not considered the radiative exchange. The species distributions of the combustion products also show good agreement. The results establish the predictive capability of the present combustion code for diffusion flame under normal gravity condition. It is assumed that the code will also predict at least qualitatively correct results at microgravity conditions with some uncertainties. This may be accepted for the basic understanding of the physical phenomena involved under this condition.

RESULTS AND DISCUSSION

Velocity and Temperature Distributions

The numerical simulation is first carried out under normal gravity and zero gravity conditions. The preliminary investigation shows that there is a huge difference in the flow pattern and in the shape of the isotherms in the two cases. The steady condition is reached approximately 0.8 s after the ignition is given. The complete steady state is achieved when there is no temporal variation around the flame as well as in the post flame zone within the solution domain. The temperature distribution in the computation domain for the diffusion flame under normal gravity condition is presented in the form of isotherms as shown in Fig. 2(a). A very high temperature gradient is observed at the base of the flame near the axis. The temperature away from the axis and near the wall is almost same as that of the inlet air or ambient air. Higher isotherms are present near the axis only.

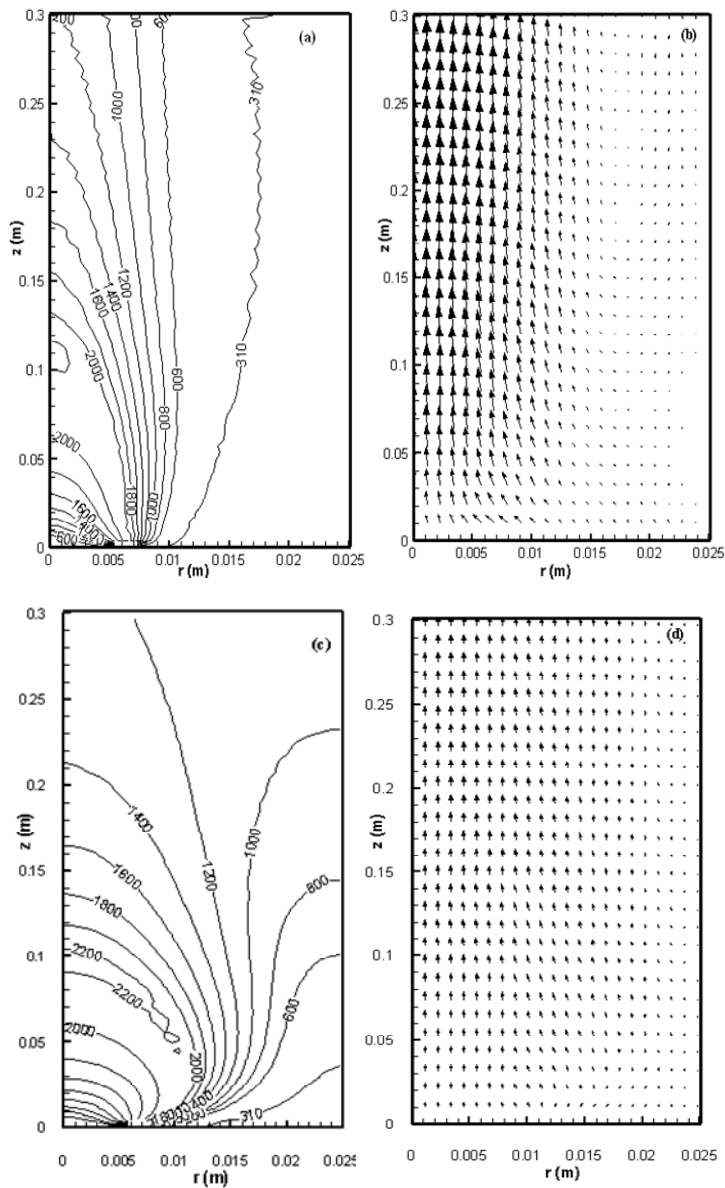


Fig. 2. (a) Temperature distributions at normal gravity, (b) Velocity distributions at normal gravity, (c) Temperature distributions at zero gravity and (d) Velocity distributions at zero gravity.

The flame structure can be further illustrated from the velocity distribution as shown in Fig. 2(b). An entrainment of flow from the co-flowing air into the flame zone is clearly indicated in the figure. The figure also reveals the acceleration in the central region due to the effects of high temperature and gravity. This further augments the entrainment process and a very high velocity, is observed in the central region within the flame. As a result of this, the pressure near the periphery drops and results in ingress of atmospheric air from the exit surface, giving rise to a recirculation zone. However, the flow velocity in the recirculation zone is very low. The recirculation zone puts a barrier to the flow of air. To satisfy the continuity equation, air at lower axial heights should entrain towards the axis of the flame.

The temperature and the velocity distributions at zero gravity are shown in figures 2(c) and 2(d) respectively. The velocity distribution shows that recirculation through the exit plane does not occur under zero gravity condition. This is due to the non-existence of buoyant force in the absence of gravity. In figure 2(c), the temperature distribution shows that the isotherms are not gathering near the axis. Rather they are uniformly distributed in the computational domain. For example, the 1000 K isotherm is seen near the wall under zero gravity condition, whereas the 1000 K isotherm is absent near the wall in the normal gravity condition.

Flame Structure

For better understanding the above difference, the flame is further simulated under different reduced gravity conditions between normal gravity (1.0 G) and zero gravity (0.0 G). The results are presented for five gravity levels including the normal and the zero gravity conditions. The structure and shape of flames under the gravity levels of 1.0 G, 0.75 G, 0.50 G, 0.25 G and 0.0 G are shown in figures 3 (a)-(e). In these figures, flame front surfaces are plotted for different gravity levels to illustrate the flame shape and flame height. The flame front is described by the volumetric heat release rate contour having value 1% of the maximum local volumetric heat release rate due to chemical reaction. In all the cases, over-ventilated flame shape is observed. It is interesting to note that the flame height decreases gradually with the decrease in gravity levels. It is approximately 11.5 cm at 1.0 G (normal) gravity level and slightly less than 10 cm at 0.0 G (zero) gravity level. This is due to the decrease of buoyant force under micro gravity condition. It is also seen that the flame is bulging slowly in the radial direction with the decrease of gravity level and become more curved at zero gravity level. The flame tip is also opening more with the decrease of gravity level.

Temperature Distribution Curves

The radial distributions of temperature at six axial positions of 2 cm, 6 cm, 10 cm, 15 cm, 20 cm and 30 cm under different microgravity conditions are presented in figures 4(a)-(f). Figure 4(a) shows that at the axial position of 2 cm, the temperature first increases upto certain radial positions and then decreases very sharply close to the inlet air temperature for all the gravity levels. But as the gravity level decreases, the radial position of the maximum temperature shifts away from the axis. The situation is more or less same at the axial height of 6 cm as shown in Fig. 4(b). The only difference is that the peak temperature becomes slightly higher (maximum by 50 K). It is expected because 6 cm is a position, which is well inside the flame. The situation becomes different at 10 cm height as shown in fig. 4(c). Here, the peak temperature position approaches the axis. Temperature propagates towards the outer wall particularly at zero gravity and also at the gravity level of 0.25G. The maximum temperature at the outer wall under zero gravity condition becomes almost 700 K and that at 0.25G is 500 K. The peak temperatures under all the gravity levels are obtained at radial position very close to the axis (approx. 2 mm away from the axis), but not exactly on the axis. Fig. 4(d) shows the radial distributions of temperature at an axial height of 15 cm. It is observed that the temperature at the centerline is the maximum in all the cases. It is also noticed that

the maximum temperatures at all the gravity levels are well below the maximum temperature as observed in the previous height already discussed. The flame height in case of axi-symmetric diffusion flame is defined as the first axial location where maximum temperature occurs on the axis of symmetry [12]. So it can be concluded that the flame height obtained from the present situation would be slightly higher than 10 cm.

The maximum centerline temperature decreases at the height of 15 cm. But significantly higher temperature of 900 K and 700 K are also seen on the wall with zero gravity and 0.25 G gravity levels. For other gravity levels the trend is same as that of normal gravity level and higher temperature is not observed adjacent to the wall. At an axial height of $z = 20$ cm [Fig. 4(e)], the difference between the centerline temperature and wall temperature decreases for zero and 0.25G gravity levels and finally at the exit plane [Fig. 4(f)], the temperature distributions become almost uniform. It is interesting to note that wall temperatures do not change much for other gravity levels. The temperature distribution in a diffusion flame is obviously related to the velocity field. The next section is all about the velocity distribution and its inter-relation with temperature distribution.

Axial Velocity Distributions

The radial distributions of axial velocity at six axial heights (2 cm, 6 cm, 10 cm, 15 cm, 20 cm and 30 cm) for different gravity levels have been shown in figures 5a-5f. It is interesting to note that the velocity distribution patterns are similar for the gravity levels of 1.0G, 0.75 G and 0.50 G whereas the patterns are

The radial distributions of axial velocity at a height of 6 cm for various gravity levels [Fig. 5(b)] show that the trend is same as that at 2 cm height. The only difference is that the velocities have increased near the central zone significantly for all the gravity levels. This fact can be explained from the presence of different amount of buoyant force at different gravity levels except at zero gravity and also the entrainment of flow towards the axis. At zero gravity, the increase in axial velocity at the centreline is due to the entrainment of flow only. At an axial height of 10 cm [Fig.5(c)], the axial velocity distribution pattern does not change much at 0.0G gravity level because of the absence of buoyant force and the velocity increases slightly due to the small acceleration provided by weak buoyant force developed there at 0.25G gravity condition. Significant change in the velocity distribution near the wall is observed with other three gravity levels considered here. There is further increase in the velocities near the axis. The velocity becomes slightly negative beyond the radial distance of 0.016 m indicating the creation of a recirculating zone near the wall.

Figure 5(d) shows that the negative velocity further increases in the recirculation zone and the corresponding centerline velocity increases for the first three gravity levels. The gradual increase of the above effect is observed at axial heights of 20 cm and 30 cm (exit plane) as shown in figures 5(e) and 5(f) respectively. This indicates that there is a large recirculation of air from the exit plane near the wall and it extends upto an axial height slightly less than 10 cm. It may be noted that the axial

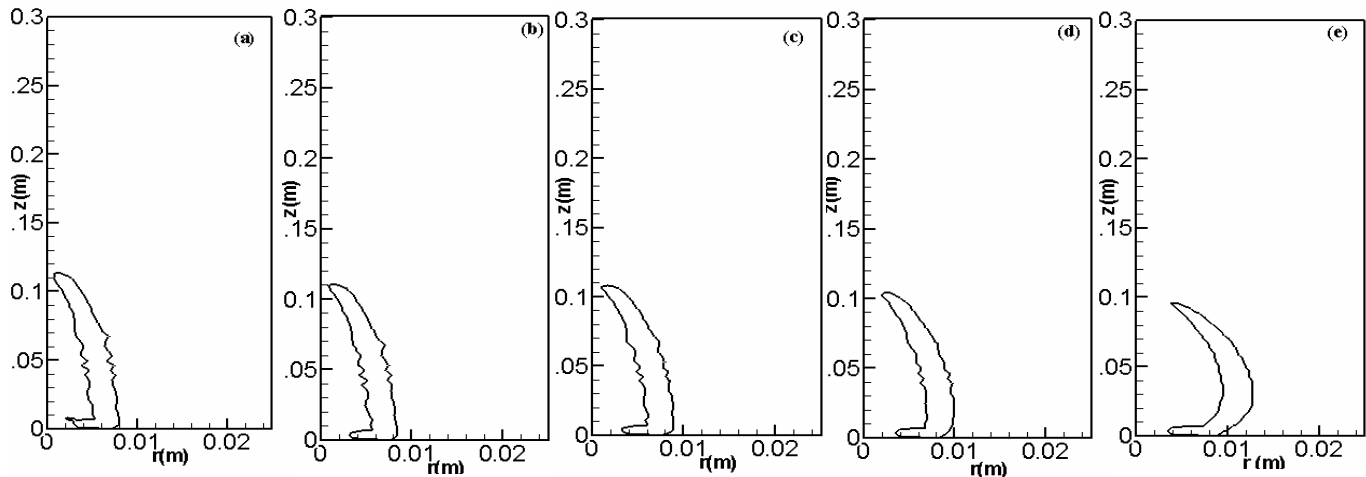


Fig.3. Flame front surface at different gravity levels: (a) 1.00 G, (b) 0.75 G, (c) 0.50 G, (d) 0.25 G and (e) 0.00 G.

of different nature at the gravity levels of 0.25G and 0.0G (zero gravity). This proves that buoyant force plays significant role in velocity distribution. Figure 5(a) shows that for all the gravity levels, maximum velocity is obtained near the centerline and this maximum velocity decrease with decrease in gravity levels. The maximum axial velocity with 1.0G is 1.20 m/s, whereas that at 0.5 G is 0.86 m/s and that at 0.0G is 0.20 m/s. Axial velocities decrease sharply beyond 0.0075 m radial distance in the gravity levels of 1.0G, 0.75G, 0.5G and 0.25G. The radial variation of axial velocity at gravity levels of 0.0 G is almost flat.

velocity never becomes negative for the gravity levels of 0.25 G and 0.0 G. This concludes that there is no recirculation of air from the exit plane due to the weak buoyant force at 0.25 G or complete absence of buoyant force at 0.0 G level.

Radial Velocity Distributions

The radial velocity distributions at different axial heights mentioned earlier are shown in Figs. 6 a-f. Figure 6(a) shows that radial velocity at an axial height of 2 cm is generally negative at all gravity levels due to the entrainment of air towards the centre.

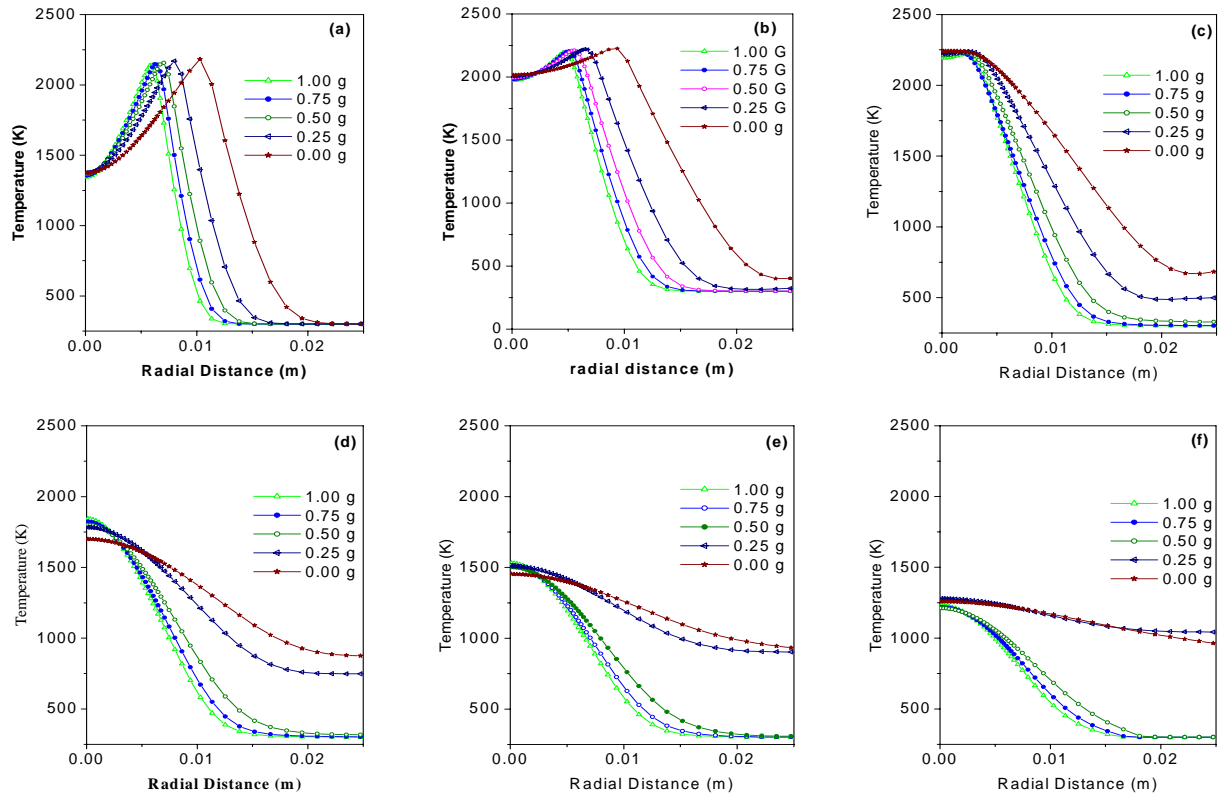


Fig. 4. Radial temperature distributions at different axial heights for different gravity levels: (a) $z = 2$ cm, (b) $z = 6$ cm, (c) $z = 10$ cm, (d) $z = 15$ cm, (e) $z = 20$ cm and (f) $z = 30$ cm.

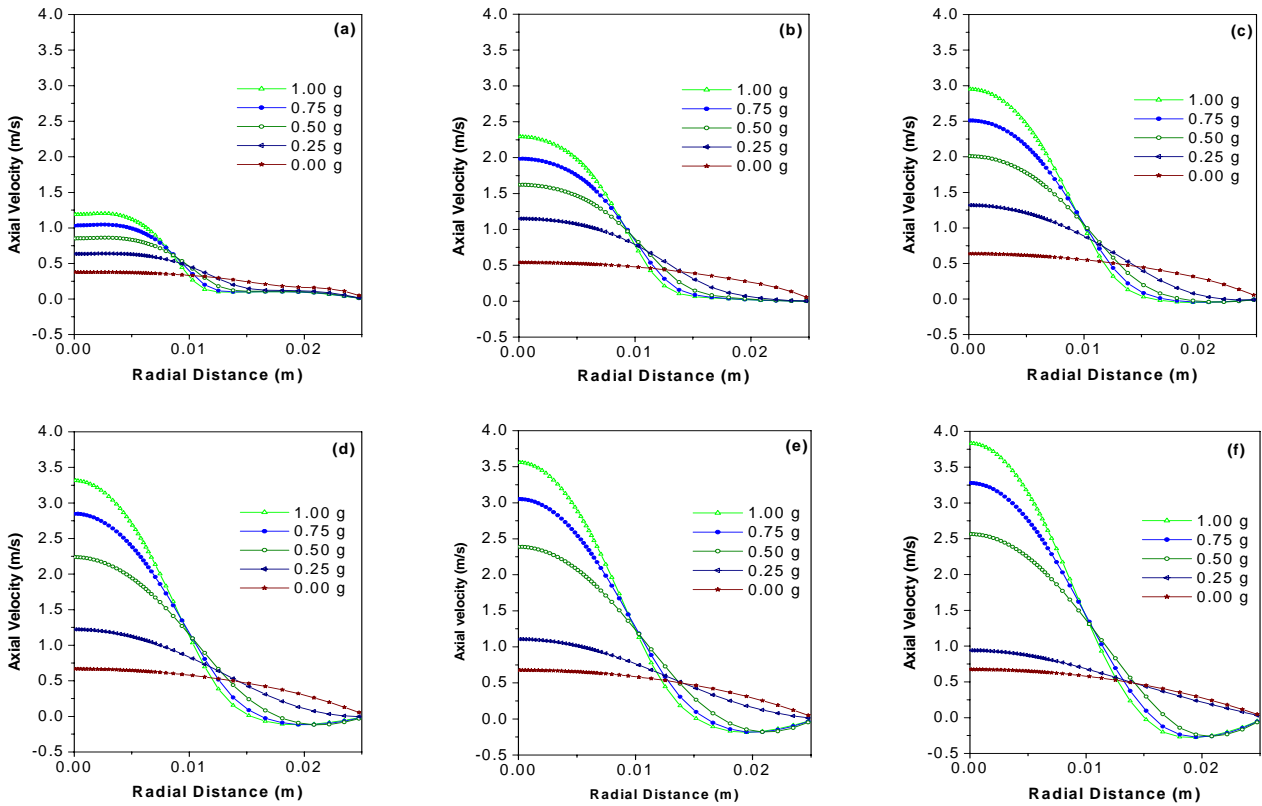


Fig. 5. Radial distributions of axial velocity at different axial heights for different gravity levels: (a) $z = 2$ cm, (b) $z = 6$ cm, (c) $z = 10$ cm, (d) $z = 15$ cm, (e) $z = 20$ cm and (f) $z = 30$ cm.

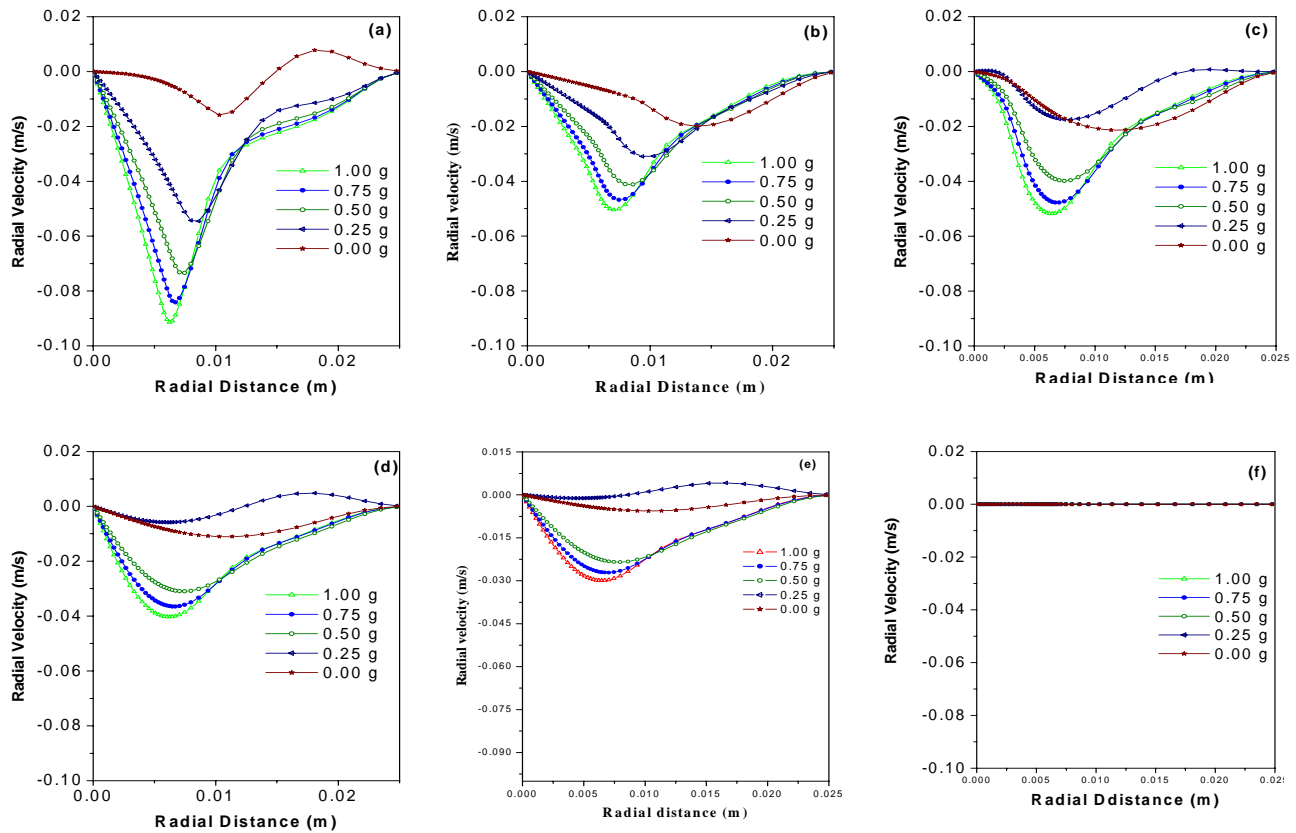


Fig. 6. Radial distributions of radial velocity at different axial heights for different gravity levels: (a) $z = 2$ cm, (b) $z = 6$ cm, (c) $z = 10$ cm, (d) $z = 15$ cm, (e) $z = 20$ cm and (f) $z = 30$ cm.

The magnitude of this negative velocity decreases with the decrease of gravity level. Of course at 0.0G (zero gravity), radial velocity is found to have positive values beyond a radial distance of 0.015 m due to partial detrainment of the gas mixture and the maximum value of this positive velocity is found to be approximately 0.00791 m/s. The negative velocity becomes maximum at around 6 to 7 mm radial position for all the gravity levels and the position of this maximum velocity shifts slightly towards the wall with decrease in gravity level. Fig. 6(b) shows that at zero gravity, the radial velocity is never positive even at a height of 6 cm and the peak value of the negative velocity decreases for all the gravity levels in comparison to the corresponding values obtained in the previous height. Figure 6(c) shows the velocity distribution pattern at an axial height of 10 cm which is almost similar to that obtained at the previous height. But the radial velocity becomes almost zero beyond a radial distance 0.016 m at gravity level of 0.25G. The reason is that there is a tendency of recirculation from the exit plane, but actually there is no recirculation due to the weak buoyant force. The radial velocity distributions at 15 cm height [Fig. 6(d)] reveal that it has positive values beyond a radial distance of 0.013 m at the gravity level of 0.25 G. This is due to the suppression of recirculation, which causes partial detrainment of the gas mixture. At other gravity levels, the patterns remain the same as observed at the previous height. The only difference is that the negative velocities in these gravity levels are slightly less than the

corresponding values in the previous height. The velocity distributions at an axial height of 20 cm [Fig. 6(e)] show some differences than that at 15 cm height. Firstly, very small amount of entrainment (i.e., very low negative velocity) of the gas is observed near the axis and detrainment starts from an earlier radial distance (approximately 0.007 m) at 0.25 G. Secondly, the magnitude of the negative radial velocity decreases further compared to the previous height at other gravity levels. Figure 6(f) shows the radial velocity, which is obviously zero for all the gravity levels.

CONCLUSION

A methane-air confined co-flowing diffusion flame has been simulated to obtain the temperature and velocity distributions within the flame and its surrounding under microgravity conditions. The gravity levels considered are 1.0G (normal gravity), 0.75G, 0.50G, 0.25G and 0.0G (zero gravity). The flame height is found to decrease with decrease in gravity level. The temperature and velocity distributions at the gravity levels of 1.0G, 0.75G and 0.50G are similar. Higher temperature zones are confined within a narrow radial distance from the axis of the flame. There is entrainment of flow at lower axial heights and a recirculation from the exit plane near the wall is also observed. The strong buoyant force at these gravity levels sets high velocity near the axis. The depth of recirculation zone decreases with decrease of gravity level. Both the velocity and temperature

distribution patterns at gravity levels of 0.25G and 0.0G are different from the above-said three gravity levels. Higher temperature zones are found to extend even upto the wall. The recirculation zone observed in the previous three cases is not formed here. This is due to either weak buoyant force (for 0.25G) or complete absence of buoyant force (for zero gravity). As a result, the increase of velocity in the central zone is also small for these two gravity levels.

NOMENCLATURE

C_j	Concentration of the j th species
c_p	Specific heat
D	Mass diffusivity
g	Acceleration due to gravity
h	Enthalpy
Le	Lewis number
p	Pressure
r	Radial distance
T	Temperature
t	Time
v	Velocity
z	Axial distance

Greek symbols

μ	Viscosity
ρ	Density
λ	Thermal conductivity

Subscript

a	Air
f	Fuel species
j	Species identification
r	Radial direction
z	Axial direction

REFERENCES

- [1] Buckmaster J., Clavin P., Linan A., Matalon M., Peters N., Siwashinsky G. and Williams F. A., "Combustion Theory and Modeling," *Proceedings of the Combustion Institute*, 2005, vol. 30, pp. 1-19.
- [2] Edelman, R. B. and Bahadori, M. Y., "Effects of Buoyancy on Gas Jet Diffusion Flames, Experiment and Theory," *Acta Astronautica*, 1987, vol. 13, pp. 681-688.
- [3] Bahadori, M. Y., Edelman, R. B., Stocker, D. P. and Olson, S. L., *AIAA J.* 28:236 (1990).
- [4] Bahadori, M. Y., Stocker, D. P. and Edelman, R. B., (1990). AIAA Paper 90-0651, 28th Aerospace Science Meeting, Reno.
- [5] Sunderland P.B., Mendelson B. J., Yuan Z. G. and D. L. Urban, "Shapes of Buoyant and Nonbuoyant Laminar Jet Diffusion Flames," *Combustion and Flame*, 1999, vol. 116, pp. 376-386.
- [6] Lin K. C., Faeth G. M., Sunderland P. B., Urban D. L. and Yuan Z.-G., "Shapes of Nonbuoyant Round Luminous Hydrocarbon/Air Laminar Jet Diffusion Flames," *Combustion And Flame*, 1999, vol. 116, pp.415-431.
- [7] Kim J., Kim K.N., Won S.H., Fujita O., Takahashi J. and Chung S.H., "Numerical Simulation And Flight Experiment On

- Oscillating Lifted Flames In Coflow Jets With Gravity Level Variation," *Combustion and Flame*, 2006, vol. 145, pp.181-193.
- [8] Lee J., Won S.H., Jin S.H., Chung S.H., Fujita O. and Ito K., "Propagation Speed of Tribachial (Triple) Flame of Propane in Laminar Jets under Normal and Micro Gravity Conditions," *Combustion and Flame*, 2003, vol. 134, pp. 411-420.
- [9] Yuan Z. G., Hegde U. and Faeth G. M., "Effects of Electric Fields on Non-buoyant Spherical Diffusion Flames," *Combustion and Flame*, 2001, vol. 124, pp. 712-716.
- [10] DuPont V., Pourkashanian M. and Williams A., "Modelling of Process Heaters Fired by Natural Gas," *Journal of Institute of Energy*, 1993, vol. 73, pp. 20-29.
- [11] Katta, V.R., and Goss, L.P. and Roquemore, W. M., "Effect of Nonunity Lewis Number and Finite Rate Chemistry on the Dynamics of Hydrogen- Air Jet Diffusion Flame," *Combustion and Flame*, 1994, vol. 96, pp. 60 - 74.
- [12] Smooke M.D., Mitchell R.E. and Keys D.E., "Numerical Solution of Two-Dimensional Axisymmetric Laminar Diffusion Flames," *Combustion Science and Technology*, 1989, vol. 67, pp. 85-122.
- [13] Reid R.C., Prausnitz J.M. and Poling, B.E., "The Properties of Gases and Liquids", *McGraw-Hill*, New York, USA. 1988.
- [14] Turns, S.R., "An Introduction to Combustion," *McGraw-Hill*, New York, USA, 1996.
- [15] Mitchell R.E., Sarofim A.F. and Clomburg L.A., "Experimental and Numerical Investigation of Confined Laminar Diffusion Flames," *Combustion and Flame*, 1980, vol. 37, pp. 227- 244.